ORIGINAL RESEARCH ARTICLE

Insight into the Viscosity–Structure Relationship of MnO–SiO_2–MgO–Al_2O_3 Fused Submerged Arc Welding Flux

ZHANJUN WANG, JIAWEN ZHANG, MING ZHONG, and CONG WANG

In this study, the influence of Al_2O_3 on the viscosity and structure of MnO–SiO_2–MgO(–Al_2O_3) submerged arc welding fluxes was investigated. The results showed that the viscosity initially decreased and subsequently increased with increasing Al_2O_3 contents from 0 to 25 mass pct, which correlates well with the "V"-shaped variation trend of the activation energy. The enhanced $(Q^2 + Q^3 + \text{Al–O}^0)/(Q^0 + Q^1 + \text{Al–O}^-)$ ratio indicated the continuous polymerization of the flux structure with higher Al_2O_3 contents, which was further confirmed by the distribution characteristics of various oxygen species. The variation trend may likely be attributed to the competing effects of the overall weakened bond energy and the enhanced degree of polymerization of the flux structure.

https://doi.org/10.1007/s11663-022-02507-4

I. INTRODUCTION

SUBMERGED arc welding (SAW) has been widely employed as one of the foremost manufacturing settings in shipbuilding, offshore engineering and pipeline manufacturing due to its exclusive advantages, such as high welding efficiency, excellent welding formability, suitable availability of automatic or semi-automatic mode, and superior reliability.[1,2] With the forthcoming application of high heat input welding, one of the ever-evolving challenges is how to ensure reliable flux detachability, weld formability and arc stability, which are related to the physicochemical properties of welding flux, especially high temperature viscosity and associated structures.[3] Furthermore, high temperature viscosity can directly affect alloying element transfer behaviors and slag-metal reactions, which eventually determine mechanical properties of the weld joints and slag detachability.[4]

Si and Mn are fundamental alloying elements in low-carbon low-alloy steels.[5] Fused SiO_2–MnO-based fluxes are favored to weld low-carbon low-alloy steels as they facilitate the release of O, Si, Mn elements under the synergistic effect of arc plasma and slag metal.[6] In addition, fluxes are typically designed with Al_2O_3, preventing SiO_2 in the flux from being reduced in the weld zone. However, only limited studies have been reported on the viscosity and structure of SiO_2–MnO-based welding fluxes. Kim *et al.*[7] investigated the viscosity and structure of the SiO_2–MnO–TiO_2 welding flux system and observed that the viscosity decreases with TiO_2/SiO_2 mass ratio and MnO content due to the limited absolute amount of SiO_2 content and also the depolymerization of the flux. According to Mysen *et al.*,[8] acidic oxides, such as SiO_2 and P_2O_5, can significantly alter the degree of polymerization of the system and form a complex silicate network. Regarding the amphoteric behavior of Al_2O_3, it generally initially exists as an acidic oxide to polymerize the network structure and increase the viscosity, and subsequently acts as a network modifier to provide O^{2-} to depolymerize the network structure and lower the viscosity.[9] However, Park *et al.*[10] observed an opposite polymerization behavior of Al_2O_3 even at high oxygen potential. Furthermore, Al-related structure also affects alloying element transfer behaviors so that Al^{3+} can substitute Si^{4+} in the silicate structure to enable sufficient Si transferred to the weld metal.[11,12] Therefore, the role of Al_2O_3 in various types of fluxes remains ambiguous, and it is still necessary to further clarify the physicochemical behavior to resolve the technical challenge in developing SiO_2–MnO-based fluxes.

In this study, the effects of Al_2O_3 on the viscous behavior of SiO_2–MnO–MgO(–Al_2O_3) flux system at various temperatures have been investigated and correlated with the flux structure. It is expected to advance the understanding of alloying element transfer behaviors

ZHANJUN WANG is with the School of Metallurgy, Northeastern University, Shenyang 110819, P.R. China and also with the State Key Laboratory of Advanced Welding and Joining, Harbin Institute of Technology, Harbin 150001, P.R. China. JIAWEN ZHANG, MING ZHONG, and CONG WANG are with the School of Metallurgy, Northeastern University. Contact e-mail: wangc@smm.neu.edu.cn

Manuscript submitted January 1, 2022; accepted March 15, 2022.
Article published online April 8, 2022.

incurred by slag-metal reactions and crystallization behaviors of the fluxes, and paving a way facilitating the design of SiO_2–MnO-based welding fluxes with desirable properties.

II. EXPERIMENTAL

A. *Sample Preparation*

All flux samples were prepared by reagent grade powders of MnO (> 99.8 mass pct), SiO_2 (> 99.7 mass pct), Al_2O_3 (> 99.8 mass pct), and MgO (>99.7 mass pct) from Sinopharm Chemical Reagent Co., Ltd., China. The detailed chemical compositions of the flux samples are shown in Table I, where the Al_2O_3 content varies from 0 to 25 mass pct and the MnO/SiO_2 mass ratio is fixed at 1. Approximately 50 g of flux samples were thoroughly mixed and placed inside a molybdenum crucible (height of 60 mm, diameter of 44 mm). The flux samples were premelted in a vertical resistance furnace at 1500 °C for 0.5 hour under the protection of high pure Ar (> 99.999 pct, 0.3 L/min) to ensure homogeneity of the melts. The premelted flux samples were then rapidly quenched by water, crushed and ground into powders. The above premelting experiment was repeated three times, and a total of nearly 150 g of samples were obtained for subsequent analysis. Chemical compositions of the premelted flux samples were analyzed by X-ray fluoroscopy (XRF, ZXS Priums II, Rigaku), as shown in Table I, where negligible changes were observed before and after premelting. Moreover, the crystalline state of the quenched flux samples was analyzed by X-ray diffraction (XRD, D8 Advance, Bruker, Germany) using a Cu Kα radiation at a voltage of 40 kV and a current of 30 mA, where the 2-theta scanning range of the XRD experiment was set between 10 and 90 deg at a scanning rate of 2 deg/min and an increment of 0.02 deg.

B. *Viscosity Measurement*

The viscosity of the flux samples was measured by the rotating cylinder method with a calibrated Brookfield digital rheometer (mold DV2T, Brookfield Engineering Laboratories). Pertinent details of the viscosity instrument and the calibration method can be found elsewhere.[13–16] A Mo crucible (height of 100 mm, diameter of 50 mm) containing 120 g pre-melted welding fluxes was placed in a vertical resistance furnace, and the flux sample was heated to 1500 °C at a heating rate of 5 °C/min. After holding 30 minutes, the viscometer was immersed into the melted flux sample according to standard procedures. Ar flow was maintained at 0.3 L/min during the process to stabilize the temperature and homogenize the flux melt. The viscosity was measured by lowering the temperature in steps of 25 °C. Each temperature was maintained for 30 minutes to achieve thermal equilibrium in the fluxes at desired temperatures. The viscosity value is the average results obtained at three different rotating rates. If the deviation of all measured experimental data from the average value is less than 3 pct, it can be confirmed that the molten flux is a Newtonian fluid at this temperature.

C. *Structural Analysis*

Fourier transform infrared spectroscopy (FTIR, Nicolet iS10, Thermal Fisher) was employed to qualitatively analyze the flux samples structure in the spectral range of 4000 to 400 cm^{-1} with a resolution of 1 cm^{-1}. Besides, semi-quantitative information of the flux sample structure was recorded by Raman spectroscopy (HR800, Horiba, Japan) in the spectral range of 400 to 1600 cm^{-1} with a resolution of 1 cm^{-1}. Furthermore, X-ray photoelectron spectroscopy (XPS, ESCALAB 250Xi, Thermo Fisher) was also used to semi-quantitatively analyze O_{1s} binding energy to detect distribution characteristics of various oxygen species. Calibration and analytical techniques of FTIR, Raman and XPS spectra can be found elsewhere.[17–19]

III. RESULTS AND DISCUSSION

A. *Crystalline States of the Quenched $MnO–SiO_2–MgO(–Al_2O_3)$ Fluxes with Different Al_2O_3 Contents*

The crystalline states of the quenched flux samples with different Al_2O_3 contents were analyzed using XRD, as shown in Figure 1. The broad diffusion peaks with amorphous characteristics in the 2-theta range of 20 to 40 deg can be observed for all the flux samples, indicating flux composition uniformity, and potentially facilitating arc stability during the welding process.[20]

B. *Effect of Al_2O_3 on the Viscosity of $MnO–SiO_2–MgO(–Al_2O_3)$ Fluxes*

Figure 2 shows the viscosity values of the flux samples in the temperature range of 1400 °C to 1500 °C, which is well in the Newtonian fluid region. It is generally believed that the viscosity of the flux at 1500 °C to 1400 °C should be in the range of 0.1–0.6 Pa s to ensure excellent weld formability during the welding process, otherwise, pocking, inferior slag detachability and other adverse phenomena may occur on the weld bead surface.[20,21] The viscosity curves of all flux samples unanimously shows V-shaped shapes, arriving at the minimum value with 15 mass pct Al_2O_3, which is inconsistent with prevailing studies focusing on the effects of Al_2O_3 content.[22–25] Al_2O_3 has been proven to exhibit amphoteric behavior, that is, with increasing Al_2O_3 content, it initially acts as a network former to promote the polymerization of the flux system and increase the viscosity; then, when the charge compensator in the flux system is insufficient, Al_2O_3 can act as a network modifier to depolymerize the flux system and lower the viscosity.[10] However, the non-monotonic tendency of viscosity demonstrated in the present study may be attributed to two factors. On the one hand, for flux samples with comparatively low content of Al_2O_3,

Table I. The Pre- and Post-experimental Compositions of the Fluxes (Mass Pct)

	Pre-experimental Composition (Weighed)				Post-experimental Composition (XRF)			
Samples	MnO	SiO_2	MgO	Al_2O_3	MnO	SiO_2	MgO	Al_2O_3
A0	47.00	47.00	6.00	0.00	48.87	45.28	5.85	0.00
A5	44.50	44.50	6.00	5.00	44.37	43.65	5.96	6.02
A10	42.00	42.00	6.00	10.00	42.21	41.06	5.98	10.77
A15	39.50	39.50	6.00	15.00	39.51	38.83	6.03	15.63
A20	37.00	37.00	6.00	20.00	38.82	35.78	5.79	19.63
A25	34.50	34.50	6.00	25.00	35.08	35.23	5.46	24.23

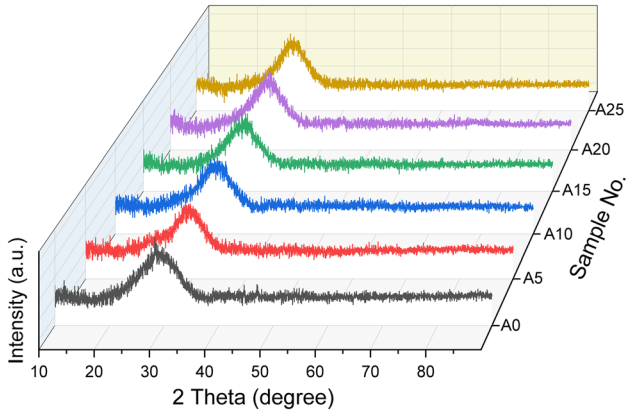

Fig. 1—XRD patterns of the quenched flux samples.

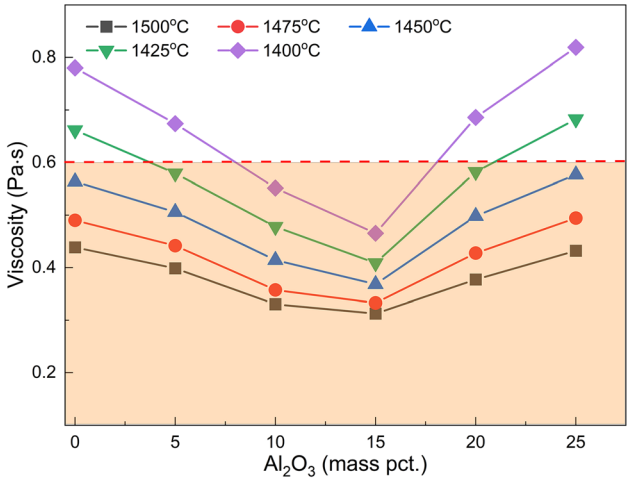

Fig. 2—Viscosities of the flux samples as a function of Al_2O_3 content at various temperatures.

the substitution of stronger Si–O bond (bond length 1.61×10^{-10} m) with weaker Al–O bond (bond length 1.75×10^{-10} m) in [(Si, Al)O_4]-tetrahedral structure and the absolute decrease content of SiO_2 may likely weaken the structure strength of the entire flux system,[26] which may lead to a decrease in the initially observed viscosity. On the other hand, with further increase of the Al_2O_3 content, more [AlO_4]-tetrahedral structural units may appear in the flux system, which requires more charge

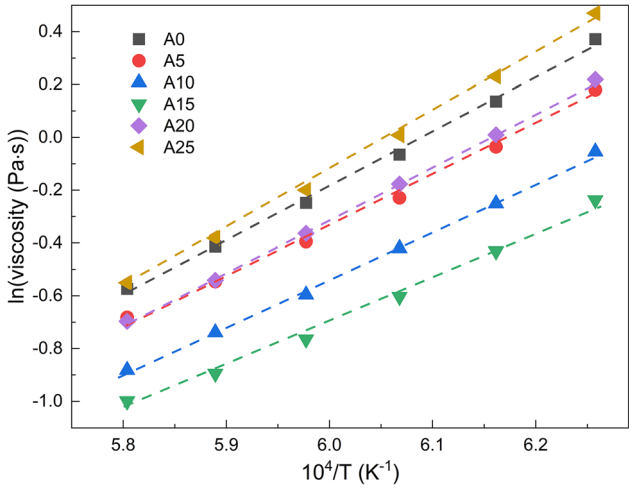

Fig. 3—Natural logarithm of viscosity (lnη) *vs* reciprocal temperature ($10^4/T$) in the Newtonian fluid region. Solid lines represent linear fitting of the data.

compensators (Mn^{2+}, Mg^{2+}), resulting in more non-bridging oxygen in the flux system to be converted into bridging oxygen to polymerize the flux system and enhance the viscosity.[27]

The activation energy (E_a) represents the frictional resistance within the structural units of the liquid flux that needs to be overcome during shearing.[16,28] For Newtonian fluids, E_a can be obtained from the Arrhenius equation,[27,29,30] as shown in Eq. [1],

$$\ln \eta = \ln \eta_0 + \frac{E_a}{R} \cdot \frac{1}{T} \qquad [1]$$

where η is the viscosity (Pa s), η_0 is a pre-exponential factor (Pa s), E_a is the activation energy for viscous flow (J/mol), T is the absolute temperature (K), and R is the ideal gas constant (8.314 J mol^{-1} K^{-1}). The liner fitting results of lnη *vs* $10^4/T$ are depicted in Figure 3 and the calculated E_a values with different Al_2O_3 contents are shown in Table II. As can be seen, E_a gradually decreases from 171.68 to 140.53 kJ mol^{-1} as the Al_2O_3 content increases from 0 to 15 mass pct and then E_a shows a significant increase from 168.05 to 187.26 kJ mol^{-1} with further addition of Al_2O_3. The specific reasons for the activation energy changes will be discussed in subsequent structural analysis section.

Table II. Activation Energy for the Viscous Flow of Different Fluxes

Sample No.	A0	A5	A10	A15	A20	A25
E_a (kJ/mol)	171.68	157.36	151.28	140.53	168.05	187.26

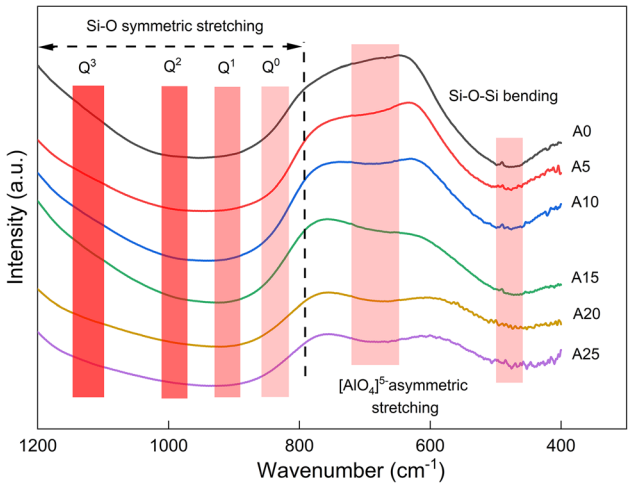

Fig. 4—FTIR spectra of flux samples with different Al_2O_3 contents.

C. *Effect of Al_2O_3 on the Structure of MnO–SiO_2–MgO(–Al_2O_3) Fluxes*

The FTIR spectra curves of flux samples with different Al_2O_3 contents are shown in Figure 4. The Si- and Al-related vibration peaks are dominant in the range of 1200 to 400 cm^{-1}, mainly including the low frequency region (550 to 400 cm^{-1}) assigned to the bending vibration of Si–O–Si bonds, the intermediate frequency region (800 to 550 cm^{-1}) allocated to the stretching vibration of $[AlO_4]$-tetrahedral units, and the high frequency region (1200 to 800 cm^{-1}) specified to the symmetrical stretching vibration of the $[SiO_4]$-tetrahedral units.[30] The gradually weakened Si–O–Si vibration in the low frequency can be attributed to two factors: one is that the decrease of the absolute content of SiO_2 leads to a reduced content of $[SiO_4]$-tetrahedral units in the flux system; the other is that the addition of Al_2O_3 promotes the transformation of Si–O–Si bonds into complex Si–O–Al bonds.[31] As a whole, the attenuating intensity of Si–O–Si vibration leads to the weakening vibration of $[SiO_4]$-tetrahedral units. Furthermore, the enhanced stretching vibration of $[AlO_4]$-tetrahedral units near ~ 700 cm^{-1} may likely imply that Si–O–Al vibration is strengthened by the copolymerization of $[AlO_4]$-tetrahedral units and $[SiO_4]$-tetrahedral units.

The original Raman spectra curves in the range of 400 to 1200 cm^{-1} for the quenched flux samples with varying involvement of Al_2O_3 are presented in Figure 5(a). Similar to FTIR results, the dominant Si–O–Si bending vibration observed between 650 and 700 cm^{-1} gradually diminishes and exhibits a higher Raman shift. The

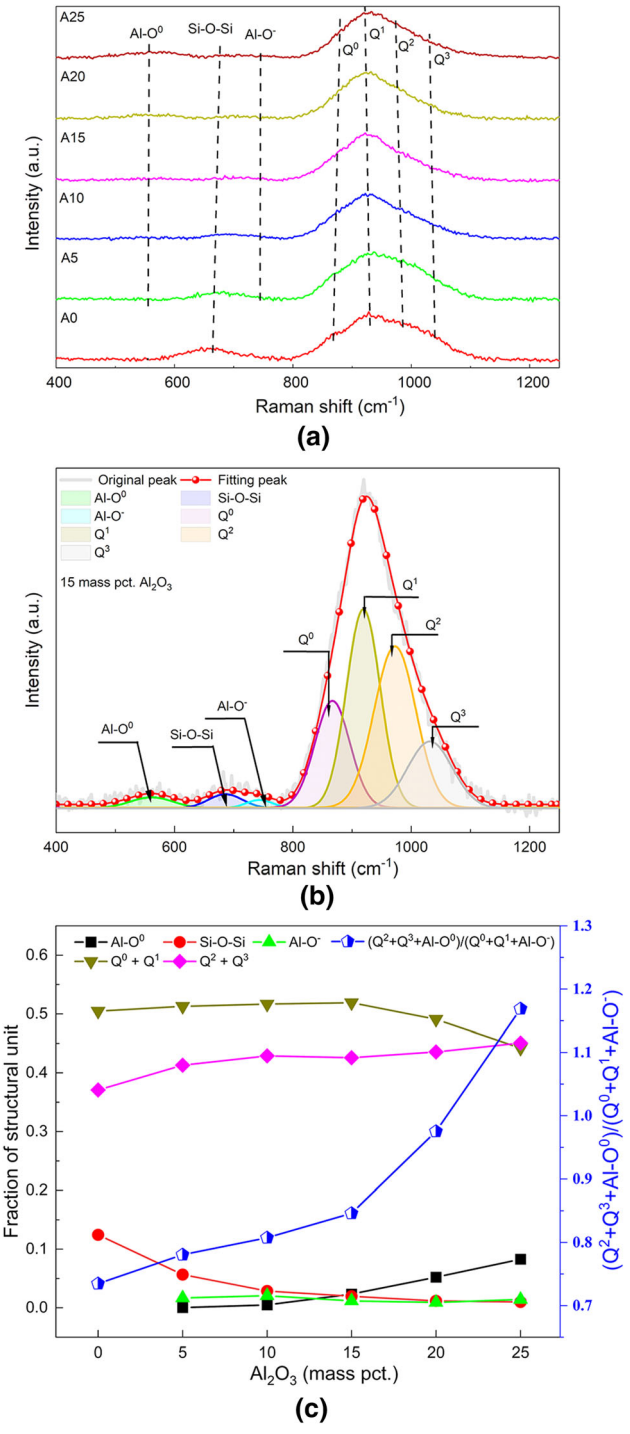

Fig. 5—(*a*) Raman spectra of welding fluxes with different Al_2O_3 contents; (*b*) typical deconvolution result of Raman spectrum; (*c*) fraction of different structural units and structural complexity with different Al_2O_3 contents.

appearance and enhancement of the stretching vibration of Al–O^- near 740 to 800 cm^{-1} and the symmetric stretching vibration of Al–O^0 at 540 to 570 cm^{-1} with higher Al_2O_3 contents indicate the formation of more complex structures.[32–34] Meanwhile, the broad vibration bands located at 800 to 1200 cm^{-1} assigned to [SiO_4]-tetrahedral units vibration become narrower with the addition of Al_2O_3, which could be owing to the fact that the vibration force constant of Al–O is smaller than that of Si–O, leading to the weakening of the coupling vibration of the entire flux structure.

To quantitatively describe the diversification of characteristic structural units, it is necessary to perform deconvolution analysis on Raman spectra to reflect all possible structures represented by different peak positions. Figure 5(b) shows the typical deconvolution results after Gaussian fitting of Raman spectra between 400 and 1250 cm^{-1}.[33,35,36] It should be mentioned that the dominant [SiO_4]-tetrahedral unit related peaks located at 800 to 1200 cm^{-1} can be divided into Q^0, Q^1, Q^2 and Q^3, respectively (Q^i, i is the number of bridging oxygen in a [SiO_4]-tetrahedral unit).[35] The area fractions of the different structural units are plotted as a function of the Al_2O_3 content and are depicted in Figure 5(c). It can be seen that the fraction of $Q^2 + Q^3$ gradually increases with increasing Al_2O_3 content, whereas that of $Q^0 + Q^1$ follows an opposite trend, indicating the polymerization of the structural units. According to the degree of aluminium avoidance rule,[37] the fraction of Al–O^0 symmetrical stretching vibration increases significantly with higher content of Al_2O_3, suggesting the transition from the silicate structure (Si–O–Si) to the more complex aluminosilicate structure (Si–O–Al).

The absence of [AlO_6]-octahedral units suggests that almost all Al_2O_3 acts as network former and consumes O^{2-} ions provided by network modifiers to form [AlO_4]-tetrahedral units. Furthermore, it should be stressed that [AlO_4]-tetrahedral units require charge compensation, implying that partial metallic cations (Mn^{2+} and Mg^{2+}) would transform from network modifiers to charge compensators, causing more non-bridging oxygen to be converted into bridging oxygen to polymerize the flux structure. According to Liang *et al.*,[35] $(Q^2 + Q^3 + \text{Al–O}^0)/(Q^0 + Q^1 + \text{Al–O}^-)$ ratio can be used to characterize the complexity of the flux structure, where the greater value represents the more complex structure and thus a higher viscosity. However, as mentioned above, although the degree of polymerization increases with the increase of Al_2O_3 content, for flux samples with Al_2O_3 contents ranging from 0 to 15 mass pct, the weaker bond energy of Al–O than that of Si–O has a dominating influence in lowering the viscosity. As for the activation energy of the viscous flow, the substitution of stronger Si–O bonds with weaker Al–O bonds would lead to a lower liquid shearing resistance of the flux after the initial addition of Al_2O_3.[26] However, the continuous increase of [AlO_4]-tetrahedral units promotes the transition of non-bridging oxygen to bridging oxygen by enhancing the degree of polymerization of the flux system, which necessitates extra energy to overcome the frictional resistance of the structural units during the shearing process.[38] In addition, according to Choi *et al.*[39] and Lee and Min,[40] the change of the main structure of the primary phase can also lead to the abrupt change of the activation energy. It can be seen from the Supplemental Materials Figure S1 that the primary phase changes from the Si-dominated structure ((Mn,Mg)SiO_4) to the Al-dominated structure ((Mn,Mg)Al_2O_4) when the Al_2O_3 content is higher than 15 mass pct, which yields an inflection point in the activation energy. Thus, a minimum activation energy value was observed for sample fluxes with 15 mass pct Al_2O_3 (Table II).

XPS analysis possesses the unique function by showcasing features of various oxygen species, including O^- (non-bridging oxygen), O^0 (bridging oxygen) and O^{2-} (free oxygen), which are closely related to the degree of polymerization of the flux structure. Figure 6(a) shows the typical deconvoluted peaks of O^-, O^0 and O^{2-} as a function of O_{1s} binding energy. The characteristic peaks

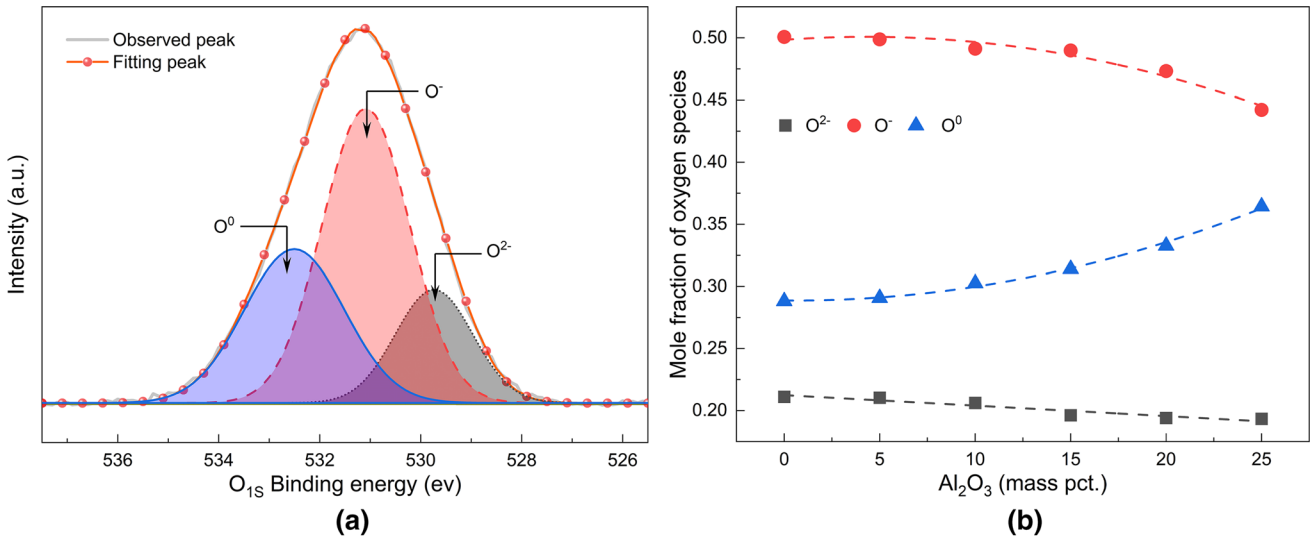

Fig. 6—(*a*) The typical deconvoluted results of O_{1S} XPS curve; (*b*) the mole fraction of various oxygen species.

of the three types of oxygens in the XPS spectra were obtained by Gaussian fitting until the R^2 value is greater than 0.994.[2,41,42] The mole fraction of various oxygen species with different Al_2O_3 contents can be calculated from the area fraction of the deconvoluted peaks, as shown in Figure 6(b). As depicted, the mole fractions of O^- and O^{2-} show a decreasing trend, whereas that of O^0 gradually increases with the increasing contents of Al_2O_3. The distribution characteristic of various oxygen species can be described by the following equilibrium reaction.[43]

$$O^{2-} + O^0 \underset{\text{depolymerization}}{\overset{\text{polymerization}}{\rightleftarrows}} 2O^- \qquad [2]$$

The increasing trend of O^0 and the decreasing trend of O^- indicate the polymerization trend of the flux structure. In addition, the formation of $[AlO_4]$-tetrahedral units would consume more Mn^{2+} and Mg^{2+} to act as charge compensators to maintain charge balance, which leads to the decrease of O^{2-}.

In short, it is demonstrated that the degree of polymerization of the flux system increases with higher Al_2O_3 content. The non-monotonic variation trend of viscosity can be ascribed to two factors: (1) when the Al_2O_3 content is within 0 to 15 mass pct, the lower bond energy of Al–O than that of Si–O has a prominent influence on decreasing viscosity; (2) when the Al_2O_3 content is ranging from 15 to 25 mass pct, the gradually enhanced degree of polymerization plays a dominant role in increasing viscosity.

IV. CONCLUSIONS

In this study, the viscosity-structure correlations of $MnO–SiO_2–MgO–(Al_2O_3)$ welding fluxes with different Al_2O_3 contents are systematically analyzed by the rotating cylinder method coupled by FTIR, Raman, and XPS techniques. Major conclusions are summarized as follows:

(1) The initial decrease and subsequent increase of viscosity and activation energy with different Al_2O_3 contents are determined by the combined effects of bond energy and degree of polymerization of the flux system.
(2) Al^{3+} ions only act as $[AlO_4]$-tetrahedral units and exhibit network former behavior. $(Q^2 + Q^3 + Al–O^0)/(Q^0 + Q^1 + Al–O^-)$ ratio increases with higher Al_2O_3 content, indicating a higher degree of polymerization of the flux structure.
(3) Increasing Al_2O_3 content can decrease the fraction of non-bridging oxygen and enhance the fraction of bridging oxygen in the flux system to polymerize the flux structure.

ACKNOWLEDGMENTS

The authors sincerely thank the National Natural Science Foundation of China (Grant Nos. 52104295, U20A20277, 51861145312, 52050410341, 52011530180), Royal Academy of Engineering (Grant No. TSPC1070), Research Fund for Central Universities (Grant Nos. N2025025, N2125016, N2125021). This work is also funded by the Regional Innovation Joint Fund of Liaoning Province (Grant No. 2020-YKLH-39) and the Open Foundation of State Key Laboratory of Advanced Welding and Joining, Harbin Institute of Technology (Grant No. AWJ-22M23).

CONFLICT OF INTEREST

On behalf of all authors, the corresponding author states that there is no conflict of interest.

SUPPLEMENTARY INFORMATION

The online version contains supplementary material available at https://doi.org/10.1007/s11663-022-02507-4.

REFERENCES

1. S.S. Shin, M. Lee, and K.H. Kim: *J. Manuf. Process.*, 2021, vol. 68, pp. 1418–29.
2. Y. Zhang, T. Coetsee, H. Yang, T. Zhao, and C. Wang: *Metall. Mater. Trans. B*, 2020, vol. 51, pp. 1947–52.
3. J.B. Kim, T.H. Lee, and I. Sohn: *Metall. Mater. Trans. A*, 2018, vol. 49A, pp. 2705–20.
4. P. Kanjilal, T.K. Pal, and S.K. Majumdar: *Weld. J.*, 2007, vol. 86, pp. 135s-s146.
5. C. Wang and J. Zhang: *Acta Metall. Sin.*, 2021, vol. 57, pp. 1126–40.
6. J.Y. Park, S.J. Park, W.S. Chang, and I. Sohn: *J. Am. Ceram. Soc.*, 2012, vol. 95, pp. 1756–63.
7. J.B. Kim and I. Sohn: *ISIJ Int.*, 2014, vol. 54, pp. 2050–58.
8. B.O. Mysen, D. Virgo, and F.A. Seifert: *Am. Mineral.*, 1985, vol. 70, pp. 88–105.
9. Y. Chen, W. Pan, B. Jia, Q. Wang, X. Zhang, Q. Wang, and S. He: *J. Non-Cryst. Solids*, 2021, vol. 552, pp. 1–8.
10. H.S. Park, S.S. Park, and I. Sohn: *Metall. Mater. Trans. B*, 2011, vol. 42B, pp. 692–99.
11. K.S. Bang, C. Park, H.C. Jung, and J.B. Lee: *Met. Mater. Int.*, 2009, vol. 15, pp. 471–77.
12. Z. Pang, X. Lv, Z. Yan, D. Liang, and J. Dang: *Metall. Mater. Trans. B*, 2018, vol. 50B, pp. 385–94.
13. J. Yang, Q. Wang, J. Zhang, O. Ostrovski, C. Zhang, and D. Cai: *Metall. Mater. Trans. B*, 2019, vol. 50B, pp. 2794–2803.
14. W. Yan, W. Chen, Y. Yang, and A. McLean: *Ironmak. Steelmak.*, 2019, vol. 46, pp. 347–52.
15. J. Li, K. Chou, and Q. Shu: *ISIJ Int.*, 2020, vol. 60, pp. 51–57.
16. Z. Wang and I. Sohn: *J. Am. Ceram. Soc.*, 2018, vol. 101, pp. 4285–96.
17. S. Lee and D.J. Min: *J. Am. Ceram. Soc.*, 2018, vol. 101, pp. 634–43.
18. W. Wang, S. Dai, L. Zhou, J. Zhang, W. Tian, and J. Xu: *Ceram. Int.*, 2020, vol. 46, pp. 3631–36.
19. D. Yang, H. Zhou, J. Wang, Z. Pang, G. Pei, Z. Yan, H. Mao, G. Qiu, and X. Lv: *J. Mater. Res. Technol.*, 2021, vol. 12, pp. 1615–22.
20. B. Singh, Z.A. Khan, and A.N. Siddiquee: *J. Mech. Eng. Res.*, 2013, vol. 5, pp. 123–27.
21. C. Wang, Z. Wang, and J. Yang: *Metall. Mater. Trans. B*, 2021, vol. 53B, pp. 693–701.

22. Z. Chen, H. Wang, Y. Sun, L. Liu, and X. Wang: *Metall. Mater. Trans. B.*, 2019, vol. 50, pp. 2930–41.
23. J. Xu, L. Su, D. Chen, J. Zhang, and Y. Chen: *J. Iron Steel Res. Int.*, 2015, vol. 22, pp. 1091–97.
24. H. Kim, H. Matsuura, F. Tsukihashi, W.L. Wang, D.J. Min, and I. Sohn: *Metall. Mater. Trans. B*, 2012, vol. 44, pp. 5–12.
25. H. Shao, E. Gao, W. Wang, and L. Zhang: *J. Am. Ceram. Soc.*, 2019, vol. 102, pp. 4440–49.
26. Z. Wang and I. Sohn: *ISIJ Int.*, 2020, vol. 60, pp. 2705–16.
27. J. Gao, G. Wen, T. Huang, P. Tang, and Q. Liu: *J. Non-Cryst. Solids.*, 2016, vol. 435, pp. 33–39.
28. M.S. Seo and I. Sohn: *J. Am. Ceram. Soc.*, 2019, vol. 102, pp. 6275–83.
29. T. Talapaneni, N. Yedla, S. Pal, and S. Sarkar: *Metall. Mater. Trans. B*, 2017, vol. 48, pp. 1450–62.
30. B.O. Mysen and M.L. Fogel: *Am. Mineral.*, 2010, vol. 95, pp. 987–99.
31. J.H. Park, H. Kim, and D.J. Min: *Metall. Mater. Trans. B*, 2008, vol. 39B, pp. 150–53.
32. W. Wang, E. Gao, L. Zhou, L. Zhang, and H. Li: *J. Iron Steel Res. Int.*, 2018, vol. 26, pp. 355–64.
33. D.A. McKeown: *Am. Mineral.*, 2005, vol. 90, pp. 1506–17.
34. H. Tian, Z. Wang, T. Zhao, and C. Wang: *Metall. Mater. Trans. B*, 2021, https://doi.org/10.1007/s1-11663-021-02359-4.
35. D. Liang, Z. Yan, X. Lv, J. Zhang, and C. Bai: *Metall. Mater. Trans. B*, 2016, vol. 48B, pp. 573–81.
36. J. Yang, J. Zhang, O. Ostrovski, C. Zhang, and D. Cai: *Metall. Mater. Trans. B*, 2019, vol. 50B, pp. 1766–72.
37. S.K. Lee and J.F. Stebbins: *Am. Mineral*, 1999, vol. 84, pp. 937–45.
38. T.S. Kim and J.H. Park: *J. Am. Ceram. Soc.*, 2019, vol. 102, pp. 4943–55.
39. J.S. Choi, T.J. Park, and D.J. Min: *J. Am. Ceram. Soc.*, 2021, vol. 104(1), pp. 140–56.
40. S. Lee and D.J. Min: *Steel Res. Int.*, 2018, vol. 89, p. 1800055.
41. G.H. Kim and I. Sohn: *J. Non-Cryst. Solids.*, 2012, vol. 358, pp. 1530–37.
42. J.H. Park and P.C.H. Rhee: *J. Non-Cryst. Solids*, 2001, vol. 282, pp. 7–14.
43. L. Wang, J. Yu, K. Chou, and S. Seetharaman: *Metall. Mater. Trans. B*, 2015, vol. 46B, pp. 1802–08.